High initial amplitude and high Mach number effects on the evolution of the single-mode Richtmyer-Meshkov instability

A. Rikanati
Department of Physics, Nuclear Research Center, Negev 84190, Israel
and Department of Physics, Ben Gurion University, Beer-Sheva 84015, Israel

D. Oron
Department of Physics of Complex Systems, Weizmann Institute of Science, Rehovot 76100, Israel

O. Sadot
Department of Physics, Nuclear Research Center, Negev 84190, Israel
and Department of Mechanical Engineering, Ben Gurion University, Beer-Sheva 84015, Israel

D. Shvarts
Department of Physics, Nuclear Research Center, Negev 84190, Israel;
Department of Physics, Ben Gurion University, Beer-Sheva 84015, Israel;
and Department of Mechanical Engineering, Ben Gurion University, Beer-Sheva 84015, Israel
(Received 3 October 2002; published 13 February 2003)

Effects of high-Mach numbers and high initial amplitudes on the evolution of the single-mode Richtmyer-Meshkov shock-wave induced hydrodynamic instability are studied using theoretical models, experiments, and numerical simulations. Two regimes in which there is a significant deviation from the linear dependence of the initial velocity on the initial perturbation amplitude are defined and characterized. In one, the observed reduction of the initial velocity is primarily due to large initial amplitudes. This effect is accurately modeled by a vorticity deposition model, quantifying both the effect of the initial perturbation amplitude and the exact shape of the interface. In the other, the reduction is dominated by the proximity of the shock wave to the interface. This effect is modeled by a modified incompressible model where the shock wave is mimicked by a moving bounding wall. These results are supplemented with high initial amplitude Mach 1.2 shock-tube experiments, enabling separation of the two effects. It is shown that in most of the previous experiments, the observed reduction is predominantly due to the effect of high initial amplitudes.

DOI: 10.1103/PhysRevE.67.026307 PACS number(s): 47.40.Nm, 47.32.−y

I. INTRODUCTION

The Richtmyer-Meshkov (RM) hydrodynamic instability [1] occurs when a shock wave passes through an initially perturbed interface between two fluids. Under such conditions, initially small perturbations on the interface grow into a formation of interpenetrating bubbles and spikes, causing the two fluids to mix. This instability, together with the gravity induced Rayleigh-Taylor instability [2], play a major role in achieving energy gain in inertial confinement fusion [3,4].

Since the first experimental demonstration of this instability by Richtmyer [1], much of the research has been focused on the evolution of single-mode small-amplitude perturbations in the incompressible limit [1,5,6]. In this regime, the perturbation initially grows with a constant velocity, which is well approximated by predictions of impulsive models: the Richtmyer formula [1] in the reflected shock case and the Meyer-Blewett formula [5] in the case of a reflected rarefaction. The model prediction for the initial velocity is

$$U_{bubble} = A^* k a^* \Delta u, \tag{1}$$

where k is the wave number, A^* is the postshock Atwood number, and Δu is the velocity jump induced by the shock wave. For the Richtmyer formula, a^* equals the postshock amplitude a_0^+ and for the Meyer-Blewett formula $a^* = (a_0^- + a_0^+)/2$, where a_0^- is the preshock amplitude. Recently, a more detailed impulsive model, applicable for both the cases of a reflected shock and a reflected rarefaction has been formulated [7].

In recent years, a more elaborate theoretical analysis of the initial velocity imprinted by the shock wave on the interface has been formulated by performing a small-amplitude perturbation expansion of the Euler equations in $a_0 k$ [8]. This approach has been extended to late nonlinear stages by means of Padé approximations [9], yielding results which are in good agreement with bubble evolution methods which are typically used to model the nonlinear stages [10]. This sort of analysis yielded results which are much more accurate than the crude approximations of the impulsive models. Indeed, it was shown that in some cases, the impulsive model prediction deviates significantly from that of the exact perturbation expansion [8]. Further extensions of the perturbative approach allow better dealing with nonlinearity [11]. This approach, however, has not been applied to the case of large initial perturbation amplitudes ($a_0 k > 1$), as is the case in many of the recent experiments.

For the single-mode case, the late nonlinear stage of the flow is characterized by an asymptotic floating velocity $c\lambda/t$. In two dimensions, c goes from $c = 1/3\pi$ for $A = 1$ [6] to $c = 1/2\pi$ for $A \to 0$ [12], while for three-dimensional perturbations c varies between $c = 1/2\pi$ for $A = 1$ and $c = 1/\pi$ for A

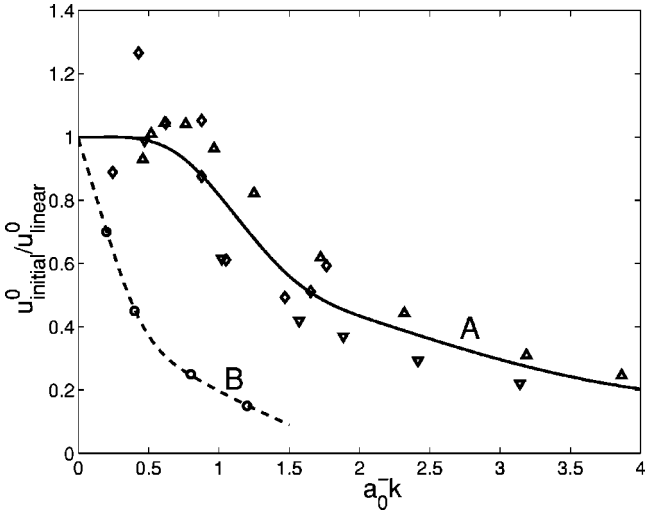

FIG. 1. Measured initial growth velocity relative to the linear extrapolation of the small-amplitude calculation. ($\diamond$) $M=15.3$ experiments of Dimonte (sinusoidal initial perturbation) [18]; ($\triangle$) $M=2.5$ Ar$\rightarrow$Xe experiments of Aleshin (sinusoidal initial perturbation) [15]; ($\bigcirc$) $M=3.5$ He$\rightarrow$Xe experiments of Aleshin (sinusoidal initial perturbation) [17]; ($\bigtriangledown$) present Mach 1.2 experiments (sawtooth initial perturbation). Schematic lines are plotted to distinguish between the two classes of behavior. ($-$) class *A* behavior, ($--$) class *B* behavior (see text).

$\rightarrow 0$ [13]. These late-time incompressible models have been verified extensively both by numerical simulations [6,12,14] and by low-Mach-number experiments [14–16].

Along with the growing complexity of the theoretical models, several experiments have been performed in recent years, in which the initial conditions greatly exceeded the limits of applicability of both small-amplitude ($a_0 k \ll 1$) and incompressible models ($M \approx 1$). Such experiments include moderate Mach shock tube experiments conducted by Aleshin *et al.* ($M=2.5$ incident shock wave, Ar$\rightarrow$Xe [15] and $M=3.5$ He$\rightarrow$Xe [17] experiments, both with an initial gas pressure of 0.5 atm) and high Mach laser driven experiments conducted by Dimonte *et al.* [$M=15.3$ incident shock wave, Be($\rho=1.7$ g/cm^3)$\rightarrow$foam($\rho=0.12$ g/cm^3) experiments [18]]. Initial amplitudes as large as $a_0 k \approx 4$, well above the limit of applicability of small-amplitude perturbation expansion, were used in these experiments. While it is commonly assumed that the deviation from small-amplitude prediction of the initial perturbation growth rate in these experiments is mainly related to compressibility effects, due to the high-Mach number [17–19], the effect of the large initial amplitude on the instability evolution seems to have been overlooked.

In this work, we attempt to distinguish between two regimes, where deviations from linear dependence of the initial imprinted velocity on the initial perturbation amplitude are observed: one where the dominant effects are those of compressibility and one which is dominated by the effects of large initial amplitudes. To do so, we first plot in Fig. 1 the measured initial growth velocity in these experiments normalized by the growth rate extrapolated from the small-amplitude calculation as a function of $a_0^- k$. Note that in all cases, where $a_0 k > 1$ the experiments resulted in an initial velocity smaller than that predicted by the small-amplitude calculation. The above velocity reduction can be attributed to two main effects: either the large initial amplitudes, for which the small-amplitude assumption is inapplicable, or compressibility effects due to the high-Mach numbers used in the experiments [17,19].

In order to better distinguish between the two effects, we conducted a set of $M=1.2$ shock-tube experiments with a similar range of initial amplitudes (a detailed description of the experiments follows below). Despite the large scatter in the experimental data, there exists a surprising resemblance of the observed reduction in the growth rate for most experiments (schematically grouped as class *A* in the figure). Only the Aleshin He$\rightarrow$Xe $M=3.5$ experiments [17] seems to exhibit a qualitatively different behavior (schematically marked as class *B*).

The qualitatively similar reduction, observed in class *A* of Fig. 1, for a wide range of Mach numbers, as low as 1.2, suggests that in these experiments, there is a strong effect of the high initial amplitude. The qualitatively different reduction observed in the Aleshin He$\rightarrow$Xe low $a_0 k$ experiment suggests the existence of a different mechanism reducing the initial growth rate.

The present work is a combined experimental and theoretical one, including numerical simulations with Mach numbers ranging from 1.2 to 15.3 with both small and large amplitudes, shock-tube experiments at Mach 1.2, a vortex deposition model for the initial velocity of the RM instability for high initial amplitudes, and a simple criterion, accounting both qualitatively and quantitatively for the different behavior observed in the group *B* experiment. As the purpose of the present work is to distinguish between effects of large amplitudes and those of compressibility, we should note that the work of Aleshin *et al.* [17], included such a characterization of shock-tube experiments (spanning a wide range of Atwood numbers—0.22–0.94, and a wide range of initial amplitudes). They termed the low-amplitude low-Mach-number region ''soft,'' the high-amplitude region ''irregular,'' and the low-amplitude high-Mach-number region ''hard.'' However, this characterization was based on the analysis of the experimental results and not on theoretical argumentation and was, therefore, less general in its applicability.

II. HIGH INITIAL AMPLITUDE EFFECTS

We have conducted full numerical simulations using the experimental setups of both Dimonte's and Aleshin's experiments, assuming ideal gas equations of state (for the Be and foam adiabatic indices of 1.8 and 1.45 were used, respectively, at an initial pressure of 0.1 Mbar). Simulations were, however, performed for a much wider range of incident shock Mach numbers (1.2–15.3). All these were conducted using LEEOR-2D, a two-dimensional hydrodynamic solver which includes interface tracking [6]. Typical results of the simulations are presented in Fig. 2 for a Mach 15.3 simulation of the Dimonte setup. The simulation results are in a very good agreement with those of Ref. [19]. Dashed

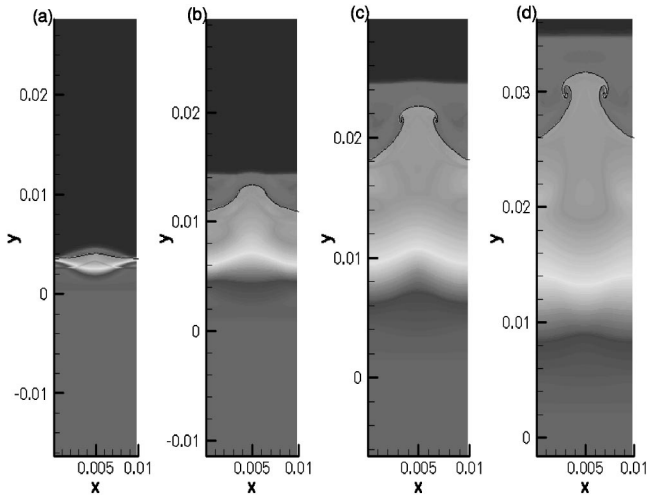

FIG. 2. Density contours from full numerical simulations of the Dimonte experiment for a Mach number of 15.3 and with $a_0k = 0.6$. (a) The incident shock, traveling upwards, hits the interface. (b)–(d) Evolution of the initial perturbation. Both the transmitted shock and the reflected rarefaction (traveling downwards) are evident.

lines in Fig. 3 show the normalized deviation from the small-amplitude linear extrapolation of the initial velocity as a function of initial amplitude for several Mach numbers. As can be seen from the simulations, a qualitatively similar reduction is observed even for low-Mach numbers where incompressible models are applicable, implying the importance of the high initial amplitudes. In the following, we describe a vorticity deposition model that, through the mechanism of shock-wave initial velocity imprint, quantifies the reduction of the initial velocity due to the high-amplitude effect.

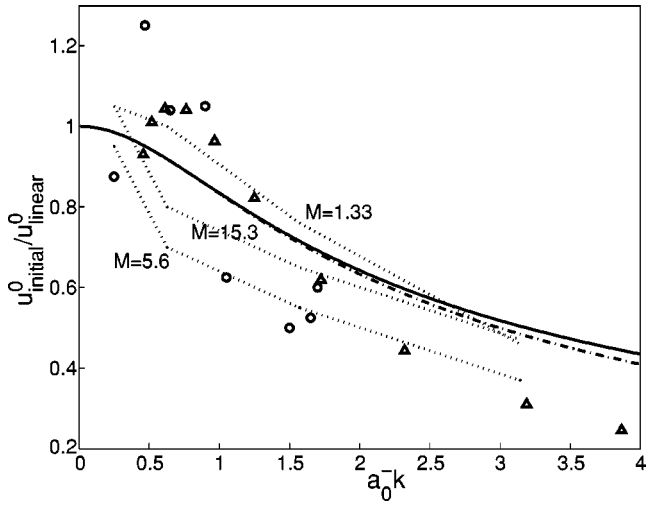

FIG. 3. Experimental, numerical and theoretical reduction factors. $(\cdots)$ numerical simulations using the Dimonte setup, the Mach numbers are indicated in the figure. $(-)$ vorticity deposition model (see text) for the Dimonte $M=15.3$ experiments. $(-\cdot-)$ vorticity deposition model for the Aleshin Ar→Xe experiments. $(\bigcirc)$ $M=15.3$ Be→foam experimental results. $(\triangle)$ $M=2.5$ Ar →Xe experimental results.

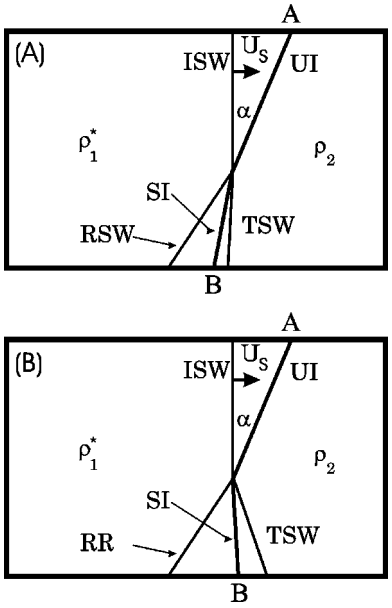

FIG. 4. Schematic description of a shock-interface interaction. (a) Fast-slow interaction, (b) slow-fast interaction. ISW—incident shock wave; TSW—transmitted shock wave; U_S—ISW velocity' UI—unshocked interface; SI—shocked interface; RSW—reflected shock wave, RR—reflected rarefaction, α—shock interface inclination angle. Also marked are points *A* and *B* on both sides of the interface (see text).

A. High initial amplitude vorticity deposition model

Using shock polar analysis, Samtaney and Zabusky [20] demonstrated that for the case of a reflected shock, the vorticity per unit length deposited on a straight interface by an oblique shock wave (see Fig. 4) is given, for angles smaller than the Mach reflection critical angle, by

$$\frac{d\Gamma}{ds} = f(M,\rho_1,\rho_2,\gamma_1,\gamma_2,p_1,p_2)\sin(\alpha) + O(\sin(\alpha)^3), \tag{2}$$

where f is a function of the one-dimensional parameters of the flow. It was also demonstrated that Eq. (2) can be extrapolated for angles beyond the critical Mach reflection angle (up to 60°), and that the local vorticity deposition on a curved interface depends only on the local impact angle and obeys Eq. (2) [20].

For the case of a reflected rarefaction, it was analytically shown in Ref. [21] that Eq. (2) is still valid, although in a more restricted range of parameters. Using Eq. (2), one can determine the vorticity deposited during the shock-wave passage through the interface in the RM experiments for an arbitrary initial shape of the interface and from that, using complex potential methods, it is possible to derive the initially imprinted bubble velocity. It should be noted that since the shock interaction with the perturbed interface is not instantaneous (i.e., point *A* in Fig. 4 moves before point *B*), the postshock perturbation amplitude decreases by a factor of $f_p=(u_{shock}-\Delta u)/u_{shock}$, where u_{shock} is the velocity of the shock wave, as illustrated in Fig. 4. This shifts the vorticity

deposited on the interface closer to the bubble tip and, therefore, affects its initial velocity.

The velocity induced due to a general periodic vorticity distribution on an interface is given by [22]

$$u(z)-iv(z)=i\int_0^{\lambda}\gamma(z)\cot\left(\frac{\pi}{2}\frac{z-z'}{\lambda}\right)dz', \tag{3}$$

where z is the complex coordinate, λ is the periodicity wavelength, and $\gamma(z)=d\Gamma/ds$ is the local vorticity on the interface. Applying the above equations for the tip of the bubble yields for the initial tip velocity,

$$u_0(a)=\mathrm{Im}[u(ia)-iv(ia)]= -\mathrm{Re}\left[\int_0^{\lambda}\frac{d\Gamma}{ds}\cot\left(\frac{\pi}{2}\frac{z-z'}{\lambda}\right)dz'\right]. \tag{4}$$

Rewriting Eq. (4) in real coordinates $[x,y(x)]$ and taking into account the amplitude change due to the shock interface interaction: $y^+(x)=f_p y^-(x)$, Eq. (2): $d\Gamma/ds=f\sin[\alpha^-(x)]$, where $\alpha^-(x)$ is the local preshock inclination angle between the interface and the incident shock, and $dz/ds=1/\cos[\alpha^+(x)]$, where $\alpha^+(x)$ is the local postshock inclination angle results in

$$u_0(a)=-\mathrm{Re}\left[f(M,\rho_1,\rho_2,\gamma_1,\gamma_2,p_1,p_2)\int_0^{\lambda}\frac{\sin[\alpha^-(x)]}{\cos[\alpha^+(x)]}\times\cot\{\pi/2[-x+iaf_p(1-y(x))]/\lambda\}dx\right]. \tag{5}$$

From Eq. (5) and depending on the initial shape of the interface (typically either sinusoidal or sawtooth), the initial velocity of the bubble tip can be found. For example, in the case of a sinusoidal initial perturbation (as in the experiments by Dimonte [18] and Aleshin [17]), the derivation results in

$$u_0(a)=-\mathrm{Re}\left[f(M,\rho_1,\rho_2,\gamma_1,\gamma_2,p_1,p_2)\int_0^{\lambda}\frac{\sin(\alpha^-)}{\cos(\alpha^+)}\times\cot\{\pi/2[-x+iaf_p(1-\cos(\pi x))]/\lambda\}dx\right] \tag{6}$$

using

$$\alpha^-=\arctan\left(\frac{dy^-(x)}{dx}\right)=\arctan[-(\pi/\lambda)a\sin(\pi x/\lambda)]$$

and

$$\alpha^+=\arctan\left(\frac{dy^+(x)}{dx}\right)=\arctan[-(\pi/\lambda)f_p a\sin(\pi x/\lambda)],$$

the integral can be solved numerically.

Rewriting Eq. (6) for small initial amplitudes ($a_0k\ll 1$), low-Mach numbers ($f_p=1$) and introducing only first-order terms, results in

$$u_0^{lin}(a)=-a\,\mathrm{Re}\left[-f\int_0^{\lambda}\pi\sin(\pi x/\lambda)\cot(-\pi/2x/\lambda)dx\right] \tag{7}$$

which is, as expected, linear in a. However, at about $a_0k>1$, higher-order terms are introduced causing deviations from linearity. We define the velocity reduction factor as $u_0(a)/u_0^{lin}(a)$. While Eq. (6) may seem intractable due to the complexity of the function f, the reduction factor turns out to be independent of it, and thus a full solution of this initial velocity is unnecessary. Calculating the reduction factor for both the Dimonte and the Aleshin Ar→Xe experiments, the parameters of the Aleshin experiment are found within the validity region of Eq. (2). Since the parameters of the Dimonte experiment are beyond this region, a numerical validation was conducted, where it was found to be valid with an error of the order of 10% for angles of up to 60° (equivalent to $a_0k=4.5$). In Fig. 3, the reduction factor is compared with both the experimental results and the numerical simulations for several Mach numbers, representing the above experiments. The agreement between the model predictions and the experiments is good. The remaining small differences between the model predictions and the numerical and experimental results might be due to high-Mach-number effects (see Sec. III). One should, however, also take into account the effect of increasing error in Eq. (2) as a_0k increases above unity, and the non-negligible dependency of the reduction factor on the initial interface shape. All these effects seem, however, small relative to the effect of high initial amplitudes.

B. High initial amplitude, low-Mach shock-tube experiments

An experimental verification of the high-amplitude effect is obtained using a shock-tube apparatus [14] at a low-Mach number of 1.2, with sawtooth initial perturbations of both low and high initial amplitudes ($a_0k=0.5$–3). In the experiments, the shock travels from air to SF_6, both initially at atmospheric pressure. The Atwood number equals to $A=0.7$. Both gases are initially separated by a thin membrane that was shown to have little effect on the instability evolution [23]. Shown in Fig. 5 is a set of Schlieren images taken from the shock-tube experiment. As described in the caption, both the bubbles and the transmitted shocks are clearly seen in the pictures. In Fig. 6, a comparison between the results from an $a_0^-k=2.4$ experiment and a simulation of the experiment is shown, with very good agreement between the two. This allows us to deduce the exact initial bubble velocity from the simulations. Figure 7 compares the experimental reduction factor with the predictions of the vorticity deposition model. As can be seen, the agreement is as good as that achieved for the moderate and high-Mach-number experiments. In addition to the above, we plot in Fig. 7 the reduction factor predicted from the vorticity model for a sinusoidal (rather than sawtooth) initial perturbation. Note that the reduction in the sinusoidal case is smaller than in the sawtooth case, similar to the difference seen in Fig. 1 between our experiment and the experiments of Dimonte and Aleshin, where the initial perturbation was sinusoidal.

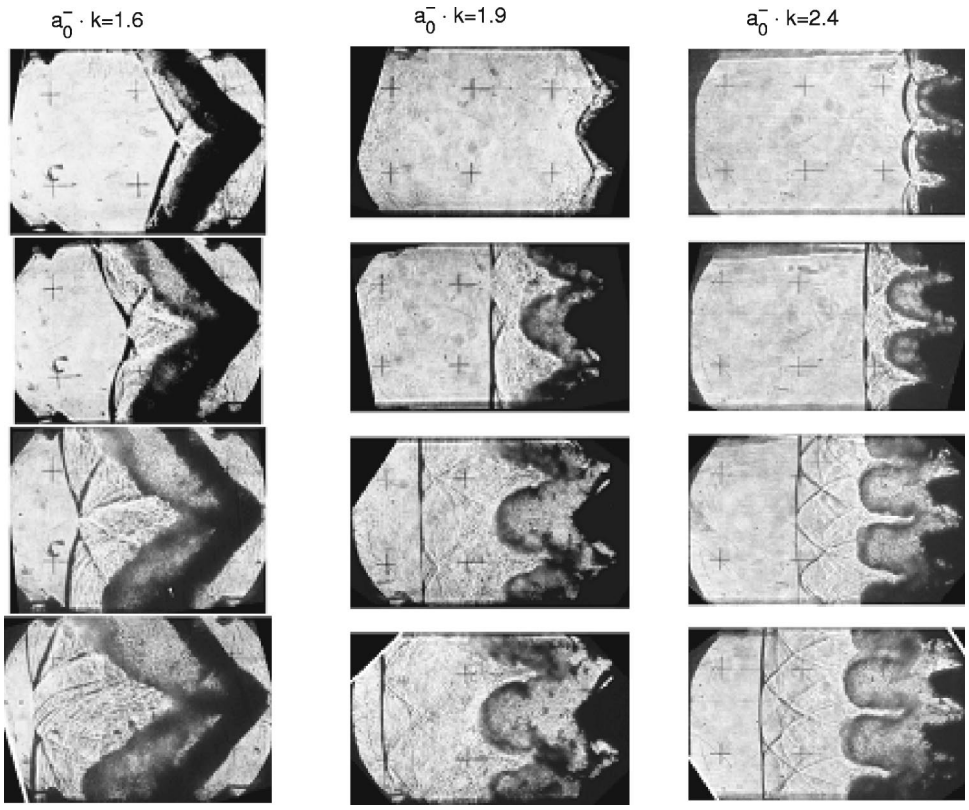

FIG. 5. Schlieren images of $M=1.2$ shock-tube experiments. Each column presents several frames from a single experiment. Both the transmitted shock wave (sharp black lines) and the bubbles (round gray features) are evident. The experiments were done with $a_0^- k = 1.6 (\lambda = 8$ cm, $a_0^- = 2$ cm), $1.9 (\lambda = 4$ cm, $a_0^- = 1.2$ cm), $2.4 (\lambda = 2$ cm, $a_0^- = 0.76$ cm), as marked in the figure. The thick black regions are the remnants of the membrane initially separating the two gases.

III. SHOCK PROXIMITY EFFECTS

As can be seen in Fig. 1, in the Aleshin He→Xe experiment [17], a decrease of the initial velocity relative to the small-amplitude calculation has been observed even for small initial amplitudes. In this experiment, the initial value of the postshock ak is smaller than unity and, therefore, the high initial amplitude effect is almost negligible. This decrease must therefore be attributed to compressibility effects. In this section, we suggest a simple criterion for determining whether such effects exist for small amplitudes. We also derive a crude, yet effective, model for evaluating the reduction factor of the initial velocity as a function of the perturbation amplitude. The model is based on *ad hoc* incorporation of the shock wave in a simple analytical incompressible model [For the sake of simplicity, the derivation assumes that the Atwood number is positive ($light \rightarrow heavy$ shock)].

The model suggests that the small-amplitude prediction is valid as long as the predicted initial velocity is much smaller than the transmitted shock velocity relative to the unperturbed interface: $u_{lin} \ll u_{shock} - \Delta u$. Moreover, the effect of

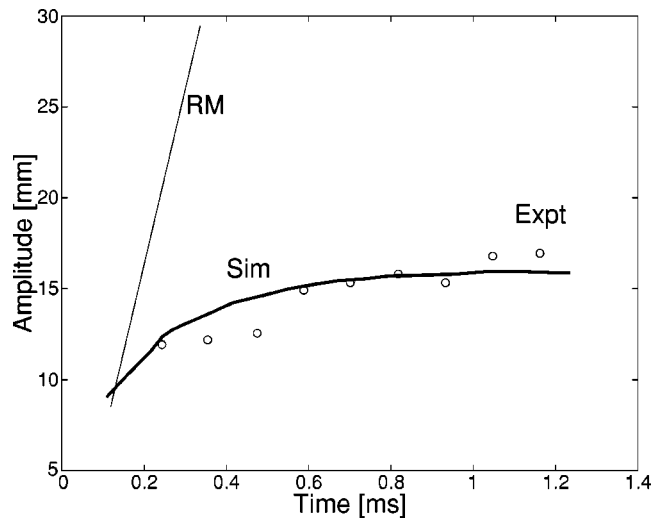

FIG. 6. The bubble height relative to the one dimensional interface as a function of time for the $a_0^- k = 2.4$ case. A comparison between the experiment (○) and the numerical simulation (−).

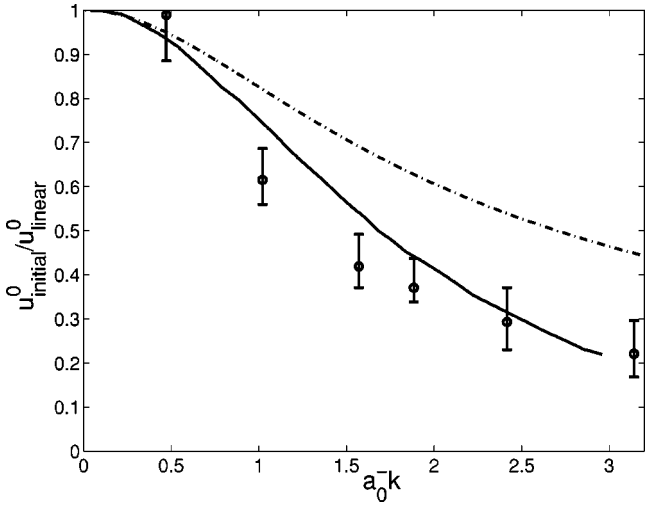

FIG. 7. Experimental reduction factor for a sawtooth initial interface (with experimental error-bars) and the theoretical reduction factor for the Mach 1.2 shock-tube experiment for a sawtooth initial interface (−) and for a sinusoidal initial interface (− · −).

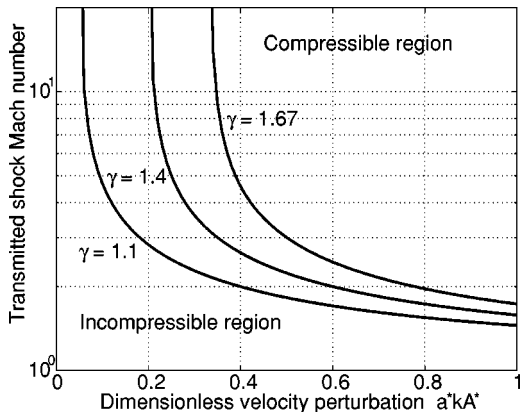

FIG. 8. Compressibility criterion for ideal gases. The $f_c=1$ contour is plotted for several adiabatic indices, γ. Regions far below and far above the lines are expected to behave in an incompressible and compressible manner, respectively.

the interaction between the shock and the interface on the initial growth rate of small initial perturbations is only dependent on the ratio $f_c=u_{lin}/(u_{shock}-\Delta u)$. Calculating f_c for the above Aleshin cases results in 0.625 and 1.25 even for the two experiments with the smallest amplitudes and, therefore, shock-wave proximity effects are expected to appear.

Assuming that the equation of state of both the materials is that of an ideal gas, f_c can be solved resulting in

$$f_c=A^*ka^*\frac{2(M^2-1)}{2+(\gamma-1)M^2}, \tag{8}$$

where M is the transmitted Mach number and γ is the heavy material adiabatic index. It should be noted that the only dependence of f_c on the light fluid parameters is through the determination of M. For this case, we plot in Fig. 8 the contour of $f_c=1$ on the initial amplitude $akA-M$ plane for several values of γ.

In attempt to incorporate the shock-wave proximity effect in a simple incompressible model and since shocked material cannot advance ahead of the shock, we model the shock wave as a ''wall'' that moves with velocity $u_{shock}-\Delta u$, bounding the bubbles from above, and inhibiting their growth. This approximation assumes that the shock velocity is unaffected by the perturbation of the interface, and is expected to provide decent results when $f_c\leqslant 1$. Despite the crudeness of this model, it is shown both to provide good quantitative predictions of the initial velocity, and to shed light on the nature of the interaction of the shock wave and the perturbed interface.

For high values of the Atwood number, we apply the generalization of Hecht *et al.* for Layzer's potential flow model for the case of a fluid layer bounded above by a wall [6] to the problem of Richtmyer-Meshkov instability evolution in the vicinity of a shock wave, where the wall location is taken as $d(t)=(u_{shock}-\Delta u)t$. In Fig. 9, a comparison between the bubble velocity from the incompressible potential model (assuming an infinite shock speed) and that of the ''wall'' model (simulating the compressible case) is seen. For the incompressible limit, it is seen that the bubble immediately reaches

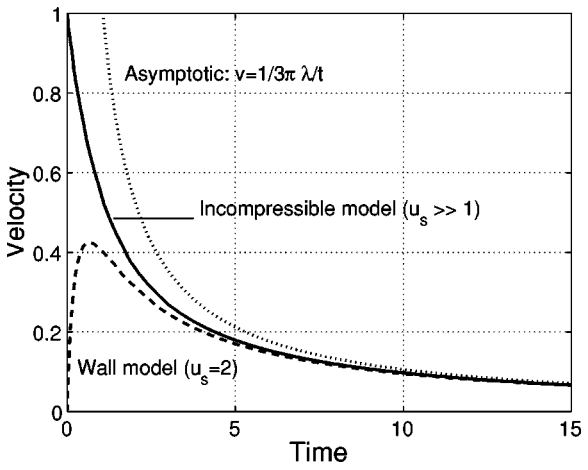

FIG. 9. Dimensionless bubble velocity (in units of u_0, the small-amplitude incompressible prediction) versus dimensionless time (ku_0t) from the potential model. A comparison between the wall model ($--$) and the incompressible potential model ($-$). Also plotted is the asymptotic value of $(1/3\pi)\lambda/t$. Notice the immediate rise in velocity for the incompressible case and that for the wall model a reduced maximal velocity (defined as the initial velocity) of 0.42 is achieved.

the velocity derived from the small-amplitude model and later decelerating until reaching the asymptotic behavior of $(1/3\pi)\lambda/t$. For a bubble bounded above by a wall, it is seen that the bubble initially accelerates from zero initial velocity in early times (when the shock wave is close to the bubble) converging to the incompressible solution as the shock wave (bounding wall) travels away from the instability front. This sort of behavior is similar to that used by Zhang *et al.* [9] in extending the perturbative approach to the nonlinear stage. We quantitatively define the reduction factor as the ratio of the maximal velocity in the wall model relative to that of the incompressible one.

For low Atwood numbers, the flow is rotational, hence potential flow models are inapplicable. Vorticity based models can, however, be applied to derive the instability evolution [12,16,24]. In the incompressible case, the instability is modeled by two counter-rotating vortex lines. A bounding wall condition is obtained by adding two more vortex lines, which are mirror images of the original vortex lines relative to the wall location. The instability evolution behaves similarly to the high Atwood number case. Due to the lower initial velocity imprinted at low Atwood numbers, it is much more difficult to achieve conditions, for which $f_c>1$ in the low Atwood range.

For both low and high Atwood numbers, the shock effect depends only on f_c since only the shock velocity relative to the bubble velocity is of importance. Hence, one can predict the dominance of the compressibility effect through the value of a single parameter of the flow, f_c.

The above wall model has been applied to predict the results of full numerical simulations of the He→Xe shock-tube experiments of Aleshin *et al.* for the cases deviating from linear dependence of the initial velocity on the perturbation amplitude (initial zero to peak amplitude of $a_0=2.5,5,10,$ and 15 mm). Since the Atwood number in these

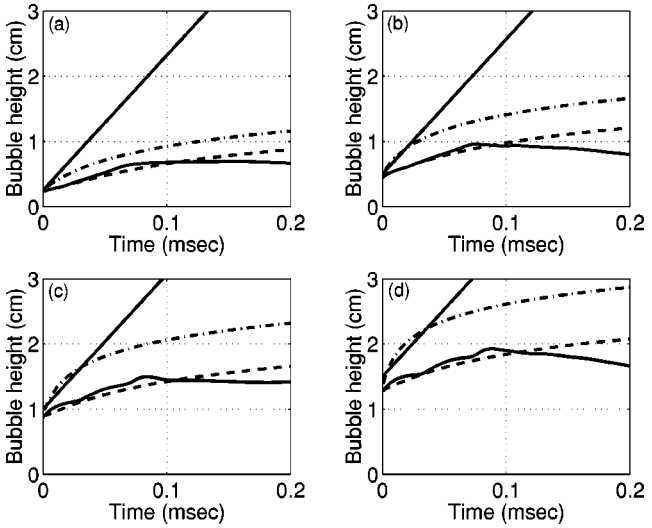

FIG. 10. Bubble height versus time representing the He→Xe Aleshin experiment from simulation (−), incompressible potential model (− · −), and wall potential model (− −). (a) $a_0k=0.43$, (b) $a_0k=0.86$, (c) $a_0k=1.72$, and (d) $a_0k=2.58$.

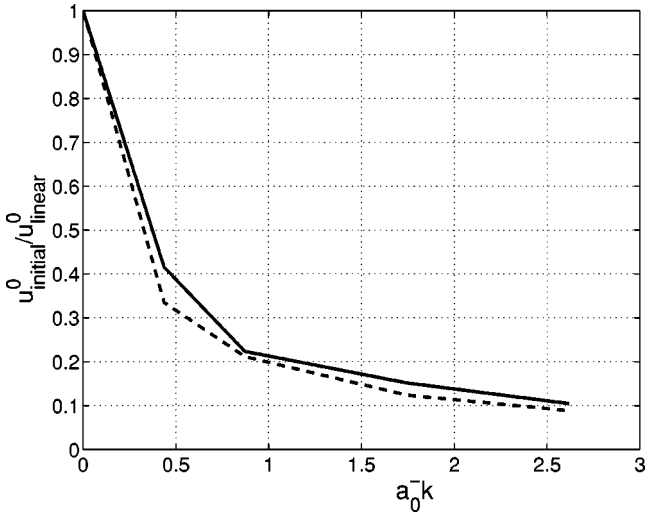

FIG. 11. Comparison of the experimental reduction factor from the Aleshin He→Xe experiments and the matching reduction factor from the potential flow wall model. The initial velocity is defined as the maximum growth velocity obtained in the early stages of the flow (see Fig. 9).

experiments is $A=0.94$, the potential model based wall model is used. In Fig. 10 are plotted the bubble heights as obtained from the simulation (found, again, to be in a good agreement with the experiment, see Fig. 2 in Ref. [17]), the incompressible potential model, and the wall model. As can be seen, the initial simulation bubble velocity is in good agreement with the wall model prediction for all the cases. In Fig. 11, one can see a comparison between the experimental reduction factor and the reduction factor predicted from the model.

However, despite the good agreement between the model and the simulation results at early times, at later times, the transverse pressure gradients created by the perturbed shock-wave structure can cause either deceleration or acceleration of the bubble and spike areas, and render this simple wall model invalid.

IV. SUMMARY

Using a combination of analytical models, experiments, and numerical simulations, we have been able to qualitatively distinguish between regimes, where deviations from linear dependence of the imprinted initial velocity on the initial perturbation amplitude are due to the large initial perturbation amplitudes or due to compressibility effects (i.e., proximity of the shock wave to the perturbed interface). These results lay a solid theoretical basis for a division to three regimes: a low-amplitude low-Mach-number regime, a high-amplitude regime, and a high-Mach-number low-amplitude regime, similar to the one derived from experimental observation by Aleshin *et al.* [17]. It was shown that the reduction in the imprinted velocity in several high-Mach-number experiments is qualitatively similar to that observed in low-Mach-number experiments with equivalent initial perturbation amplitudes. A vorticity deposition model that describes the effects of high initial amplitudes as well as those of the interface shape, and a modified potential model describing effects of shock proximity, both predicting a reduction in the initial bubble velocity, in good agreement with previous experimental results are presented. These are supplemented by new shock-tube experiments and full numerical simulations. We believe that these findings will be of use in attempting to analyze and quantify the instability evolution in complex cases where both compressibility and high initial amplitude effects are observed.

ACKNOWLEDGMENTS

The authors wish to thank Professor Dan Meiron for helpful discussions and the Department of Applied Mathematics at CalTech and the Laboratory for Laser Energetics at the University of Rochester for their hospitality and partial support during this work.

[1] R.D. Richtmyer, Commun. Pure Appl. Math. **13**, 297 (1960); E.E. Meshkov, Fluid Dyn. **4**, 101 (1969).
[2] Lord Rayleigh, Proc. London Math. Soc. **14**, 170 (1883); *Scientific Papers* (Cambridge University Press, Cambridge, 1900), Vol. 2, p. 200.
[3] J.D. Lindl, Phys. Plasmas **2**, 3933 (1995).
[4] S.W. Haan, Phys. Plasmas **2**, 2480 (1995).
[5] K.M. Meyer and P.J. Blewett, Phys. Fluids **15**, 753 (1972).
[6] J. Hecht, U. Alon, and D. Shvarts, Phys. Fluids **6**, 4019 (1994); U. Alon, J. Hecht, D. Mukamel, and D. Shvarts, Phys. Rev. Lett. **72**, 2867 (1994); U. Alon, J. Hecht, D. Ofer, and D. Shvarts, *ibid.* **74**, 534 (1995).

[7] M. Vandenboomgaerde, C. Mugler, and S. Gauthier, Phys. Rev. E **58**, 1874 (1998).
[8] Y. Yang, Q. Zhang, and D.H. Sharp, Phys. Fluids **6**, 1856 (1994).
[9] Q. Zhang and S.I. Sohn, Phys. Fluids **9**, 1106 (1997).
[10] D. Layzer, Astrophys. J. **22**, 1 (1955).
[11] M. Vandenboomgaerde, S. Gauthier, and C. Mugler, Phys. Fluids **14**, 1111 (2002).
[12] A. Rikanati, U. Alon, and D. Shvarts, Phys. Rev. E **58**, 7410 (1998).
[13] D. Oron, L. Arazi, D. Kartoon, A. Rikanati, U. Alon, and D. Shvarts, Phys. Plasmas **8**, 2883 (2001).
[14] O. Sadot, L. Erez, U. Alon, D. Oron, L.A. Levin, G. Erez, G. Ben-Dor, and D. Shvarts, Phys. Rev. Lett. **80**, 1654 (1998).
[15] A.N. Aleshin, E.V. Lazareva, S.G. Zaitsev, V.B. Rozanov, E.G. Gamali, and I.G. Lebo, Sov. Phys. Dokl. **35**, 159 (1990).
[16] J.W. Jacobs and J.M. Sheeley, Phys. Fluids **8**, 405 (1996).
[17] A. N. Aleshin, E. V. Lazareva, E. I. Chebotareva, S. V. Sergeev, and S. G. Zaytsev, in *Proceedings of Invited Papers, of the Sixth International Workshop on Compressible Turbulent Mixing, Marseille, 1997*, edited by G. Jourdan and L. Houas (IUSTI Universitè de Provence, France, 1997), p. 1.
[18] G. Dimonte, C.E. Frerking, M.B. Schneider, and B. Remington, Phys. Plasmas **3**, 614 (1996).
[19] R.L. Holmes, G. Dimonte, B. Fryxell, M.L. Gitting, J.W. Grove, M. Schnider, D.H. Sharp, A.L. Velikovich, R.P. Weaver, and Q. Zhang, J. Fluid Mech. **389**, 55 (1999).
[20] R. Samtaney and N.J. Zabusky, Phys. Fluids A **5**, 1285 (1993).
[21] R. Samtaney, J. Ray, and N.J. Zabusky, Phys. Fluids **10**, 1217 (1998).
[22] G.R. Baker, D.I. Meiron, and S.A. Orszag, Phys. Fluids **23**, 1485 (1980).
[23] L. Erez, O. Sadot, D. Oron, G. Erez, L.A. Levin, D. Shvarts, and G. Ben-Dor, Shock Waves **10**, 241 (2000).
[24] N. Zabusky, J. Ray, and R. S. Samtaney, in *Proceedings of Invited Papers, of the Fifth International Workshop on Compressible Turbulent Mixing, Stony Brook, 1995*, edited by R. Young, J. Glimm, and B. Boyton (World Scientific, Singapore, 1996), p. 89.